Geological Society of Norway

Relative permeability and residual gaseous CO_2 saturation in the Jurassic Brentskardhaugen Bed sandstones, Wilhelmøya Subgroup, western central Spitsbergen, Svalbard

Javad Naseryan Moghadam[1], Mohammad Nooraiepour[1], Helge Hellevang[1,2], Nazmul Haque Mondol[1,3] & Per Aagaard[1]

[1]*Department of Geosciences, University of Oslo (UiO), P.O. Box 1047 Blindern, 0316 Oslo, Norway.*
[2]*The University Centre in Svalbard (UNIS), P.O. Box 156, 9171 Longyearbyen, Norway.*
[3]*Norwegian Geotechnical Institute (NGI), P.O. Box 3930 Ullevaal Stadion, 0806 Oslo, Norway.*

E-mail corresponding author (Mohammad Nooraiepour): mohammad.nooraiepour@geo.uio.no

This study investigates fluid-flow properties of the low-permeability Brentskardhaugen Bed (Knorringfjellet Formation), Wilhelmøya Subgroup, western central Spitsbergen, Svalbard. To evaluate the two-phase relative permeability of the water-CO_2 system, we performed unsteady state core-flooding experiments using deionised water and gaseous CO_2. The absolute permeability and residual fluid saturations were also studied. Moreover, a core plug of the Berea sandstone was tested as a reference sample. The core-flooding experiments recorded microDarcy permeability values (0.022–0.039 mD) for various differential pressures (4 to 12 MPa). The poor grain sorting and the abundance of cement were the main factors controlling the low matrix permeabilities. Closure of sub-micron fractures was the likely reason for reduced permeability with increasing effective stresses. The experimental measurements showed that CO_2 fractional flow reached unity at relatively low CO_2 saturation (approximately 0.35–0.45). The irreducible water saturation and trapped CO_2 saturation were 56% and 23%, respectively. The corresponding endpoint CO_2 and water relative permeability were 0.18 and 0.47, respectively. The results, therefore, demonstrate low endpoint CO_2 saturation and low relative permeability, in addition to high CO_2 fractional flow at high water saturation. The trapped CO_2 saturation was relatively high, which suggests a high CO_2 immobilisation capability of the Wilhelmøya Subgroup sandstones. Moreover, a lower relative permeability was observed for gaseous CO_2 compared to published results for supercritical CO_2. In addition, the examined core sample showed a higher trapped CO_2 saturation and higher endpoint CO_2 relative permeability compared with the porous and permeable Berea sandstone.

Keywords: relative permeability, residual CO_2 saturation, Knorringfjellet Formation, Longyearbyen CO_2 storage pilot, geological CO_2 sequestration

Received 8. August 2018 / Accepted 5. November 2018 / Published online 24. February 2019

Introduction

Geological CO_2 sequestration is recognised as an essential measure with substantial potential for reducing atmospheric emissions of carbon dioxide (CO_2). CO_2 storage requires storage reservoirs with sufficient storage capacity and stratigraphic or structural seals that prevent the buoyant CO_2 from escaping the reservoir. High-porosity and high-permeability reservoirs are desired, but also unconventional reservoirs, with a low permeability matrix but with significant storage capacity in fracture networks, should be considered if the reservoir is placed favourably to CO_2 point sources and other infrastructures required for a CO_2 storage operation, such as the Krechba site, Algeria (Iding & Ringrose, 2010; Rinaldi & Rutqvist,

Moghadam, J.N., Nooraiepour, M., Hellevang, H., Mondol, N.H. & Aagaard, P. 2018: Relative permeability and residual gaseous CO_2 saturation in the Jurassic Brentskardhaugen Bed sandstones, Wilhelmøya Subgroup, western central Spitsbergen, Svalbard. *Norwegian Journal of Geology 98*, 1–12. https://dx.doi.org/10.17850/njg005.

2013). The UNIS CO_2 Laboratory, Longyearbyen, Svalbard, Norway, offers detailed characteristics of such an unconventional, dual-permeability, dual-porosity, CO_2 storage site (Sand et al., 2014 and references therein). Data from the UNIS CO_2 Laboratory includes eight drillholes with a total length of about 4.5 km, detailed investigations of reservoir and seal properties from cores and field outcrops, wireline logs, 2D seismic among other datasets (Sand et al., 2014). The reservoir sand with the best properties was found in the Upper Triassic to Middle Jurassic Wilhelmøya Subgroup, having porosities between 1 and 18% and with absolute permeability < 7 mD (Braathen et al., 2012; Mørk, 2013; Magnabosco et al., 2014; Van Stappen et al., 2014; Bultreys et al., 2016). The relative permeability of CO_2 in these water-wet sandstones was not measured but instead numerically simulated using pore network models (PNMs) based on a geometry obtained from high-resolution CT scans of cored materials (Van Stappen et al., 2014; Bultreys et al., 2016). Van Stappen et al. (2014) suggested relative CO_2 permeabilities of 0.43 and 11 mD for two selected samples, but the authors noticed that these values are probably too high when comparing with the laboratory measurements of absolute permeability. This was also confirmed in a later study where the matrix permeability was found to be < 1 mD for selected samples from the De Geerdalen Formation (Van Stappen et al., 2018). The permeabilities were found to decrease exponentially with confining pressure, confirming the dominance of the fracture flow and suggesting that fracture aperture closing was the main mechanism reducing the permeabilities (Van Stappen et al., 2018). Pore-scale simulations furthermore suggested high residual CO_2 saturation of the selected samples, at 50% and 59% respectively, after an imbibition cycle (Van Stappen et al., 2014). Finally, the authors noted that the fracture density increased when they increased the spatial CT-scanner resolution, suggesting that sub-micron fractures could connect pores and affect the fluid flow in the samples (Van Stappen et al., 2014).

The relationship between the relative permeability and the saturation of the non-wetting phase is well known and varies as a function of parameters such as rock composition, grain architecture, and fracturing (Krevor et al., 2012). During the migration of injected CO_2, drainage and imbibition processes occur within the storage reservoirs. As the CO_2 front advances through the drainage stage, the in situ pore-water saturation decreases. When the wetting phase (water) during imbibition re-enters the pore volume at the edges of the migrating CO_2 plume, it disconnects and immobilises the trapped CO_2 bubbles. As a result, CO_2 relative permeability becomes zero when there is still a notable fraction of the CO_2 saturation present within the pore space. This is referred to as the residual trapping mechanism. Experimental investigations documented a maximum trapped CO_2 saturation of 40% when saturation of CO_2 reached 60–80% during core-flooding experiments (Pentland et al., 2011; Krevor et al., 2012; Pini et al., 2012; Akbarabadi & Piri, 2013; Ruprecht et al., 2014). The residual trapping, in turn, affects the distribution of the CO_2 plume (Juanes et al., 2006; Krevor et al., 2012) and determines how far the injected CO_2 migrates (Doughty, 2007; Qi et al., 2009; Burnside & Naylor, 2014). The residual trapping is a rapid immobilisation mechanism, which occurs over time scales of days in core-flooding experiments (Pentland et al., 2011; Shi et al., 2011), and is anticipated to contribute significantly to CO_2 entrapment within a decade (Sifuentes et al., 2009; Saadatpoor et al., 2010). Capillary pressure characteristics and water-CO_2 relative permeability control the mobile and immobile phases during CO_2 sequestration. A knowledge of relative permeability is also necessary for engineering estimates and modelling purposes to evaluate more accurately the fate of injected CO_2.

This paper presents measured relative permeabilities of gaseous CO_2 on a selected plug sample from the Wilhelmøya Subgroup from borehole DH4. Because the reservoir units in the Longyearbyen CO_2 Laboratory pilot show significant underpressure (approximately 30% of hydrostatic pressure according to Braathen et al., (2012)), we performed the relative permeability measurements using a gaseous CO_2 phase state. To evaluate fluid-flow properties, we measured matrix permeability and two-phase relative permeability of the deionised water-gaseous CO_2 system. The experimental results were also compared with several published relative permeability models to investigate whether these correlations can be used to describe water-CO_2 flow properties of the Wilhelmøya Subgroup. The obtained relative permeabilities were finally compared with earlier measured and simulated data. The research results may provide a better understanding of CO_2 flow properties in unconventional tight sandstones with potential sub-micron fractures affecting the CO_2 flow and residual CO_2 trapping.

Materials and methods

Reservoir and core sample properties

The sandstone sample was taken from the Brentskardhaugen Bed at a depth of 674.79 m in borehole DH4, a 969.8 m-deep vertical well drilled as a part of the pilot study at the UNIS CO_2 Lab. The Bathonian Brentskardhaugen Bed is the uppermost unit of the Upper Triassic to Middle Jurassic Wilhelmøya Subgroup (Mørk et al., 1999). In western and central Spitsbergen the subgroup consists of a condensed, approximately 20 m-thick, mixed sandstone-shale unit with subordinate polymict conglomerates and defined as the Knorringfjellet Formation (Mørk et al., 1999). The Brentskardhaugen Bed contains Toarcian, Aalenian and Bajocian reworked fossils (Bäckström & Nagy, 1985) and in this area consists of an up to 4 m-thick, matrix- to grain supported, polymict to monomict, phosphate conglomerate interbedded with fine- to coarse-grained sandstones with scattered glauconite grains (Rismyhr et al., this volume).

In this study, we also used the Mississippian Berea sandstone as a reference core sample because several CO_2-brine relative permeability studies have been performed on this sandstone before (for example, Pini et al., 2012; Benson et al., 2013; Chen et al., 2014). The Berea is a medium- to fine-grained and well-sorted subarkosic arenite (Table 1) that is widely used as reference material for geological and petroleum engineering research (for instance Oak et al., 1990; Tidwell & Wilson, 1999; Moore et al., 2004; Krevor et al., 2012).

Sample preparation and characterisation

The mineralogical composition including bulk (whole-rock) and clay mineral fractions was identified and quantified using the X-ray diffraction (XRD) technique. The details of XRD sample preparation and analysis are presented in Nooraiepour et al. (2017a, b). The studied core plug was also characterised using optical microscopy of polished thin-sections stained blue to show porosity, and supplemented by scanning electron microscopy (SEM). SEM analyses and backscatter electron imaging (BEI) with energy-dispersive x-ray spectroscopy (EDS) were also included for mineral identification and microstructural interpretation. A Hitachi SU5000 FE-SEM (Schottky FEG) provided the SEM analyses, and the EDS was performed on a Dual Bruker XFlash system and an HR EBSD system.

Experimental set-up

In this study, we used a high-pressure, high-temperature, AFS 200 core flooding system (Core Laboratories). Figure 1 shows a schematic presentation of the experimental set-up. The core flooding system is equipped with a forced convection benchtop oven (Despatch LBB series), which combines horizontal and vertical airflow, and provides temperature uniformity within the air bath. The system is designed to perform unsteady-state relative permeability experiments. The fluid injection system comprises one dual-cylinder syringe pump (Teledyne Isco, 100DM), which controlled the flow of brine and CO_2. A back-pressure regulator and a single-cylinder syringe pump (Teledyne Isco, 500D) control the fluid pressure inside the system. Two stainless steel accumulators within the benchtop oven allow us to equilibrate brine and CO_2 phases before the injection. The core flooding system is equipped with a Hassler-type stainless steel core holder and a two-phase separator. The built-in distribution plugs within the end caps of the core holder distribute the injected fluid evenly at the inlet and the outlet. The injected fluid passes through the separator, and the liquid outlet can be measured by either a built-in separator or a mounted high-precision digital scale. Three gas mass-flow controllers, at three different working ranges, detected CO_2 flow after the back-pressure regulator. Two sets of pressure transducers monitor fluid pressure at the inlet and outlet of the core holder. The core flooding system allows for automated management of hardware resources, data acquisition and recording. High-pressure steel tubing, fittings and valves were used for plumbing inside the experimental system.

Experimental procedure

We performed core-flooding experiments using gaseous CO_2 and deionised water (Milli-Q water) to determine absolute permeability and relative permeability. To avoid precipitation of salt crystals and following changes in properties of the porous medium, deionised water (DI-water) was used instead of brine. All the experiments were carried out at the room temperature of 21–23°C. The geochemical reactions between the rock and injected fluids were considered unlikely at the experimental time scale and pressure–temperature conditions. Even the occurrence of such potential reactions under the present experimental conditions would have resulted in insignificant changes in the pore space and, thus, in any permeability measurements.

Absolute permeability measurement

To measure absolute permeability, we performed steady-state flooding tests at constant pressure gradient conditions and calculated permeability using Darcy's law. In these flow measurements, while pore pressure was kept constant in each cycle (2, 3 and 4 MPa), the confining pressure was increased stepwise (1 MPa increments) up to 16 MPa. The pore pressure was calculated as the average of fluid pressure at the inlet and the outlet. The Klinkenberg correction (Klinkenberg, 1941; Civan, 2010) was applied for the CO_2 permeability measurements. For a detailed procedure, the reader is referred to Moghadam et al. (2016) and Nooraiepour et al. (2018a).

Table 1. *Mineralogical composition of the tested core plugs (in percentage).*

Core plug	*Total porosity*	*Quartz*	*Feldspar*	*Siderite*	*Pyrite*	*Clay minerals*		
						Chlorite	*Illite/Muscovite*	*Kaolinite*
Brentskardhaugen Bed Sandstone	10.5	66.30	4.40	11.30	0.10	15.50	1.80	0.60
Berea	21	90.71	4.53	-	-	-	-	4.76

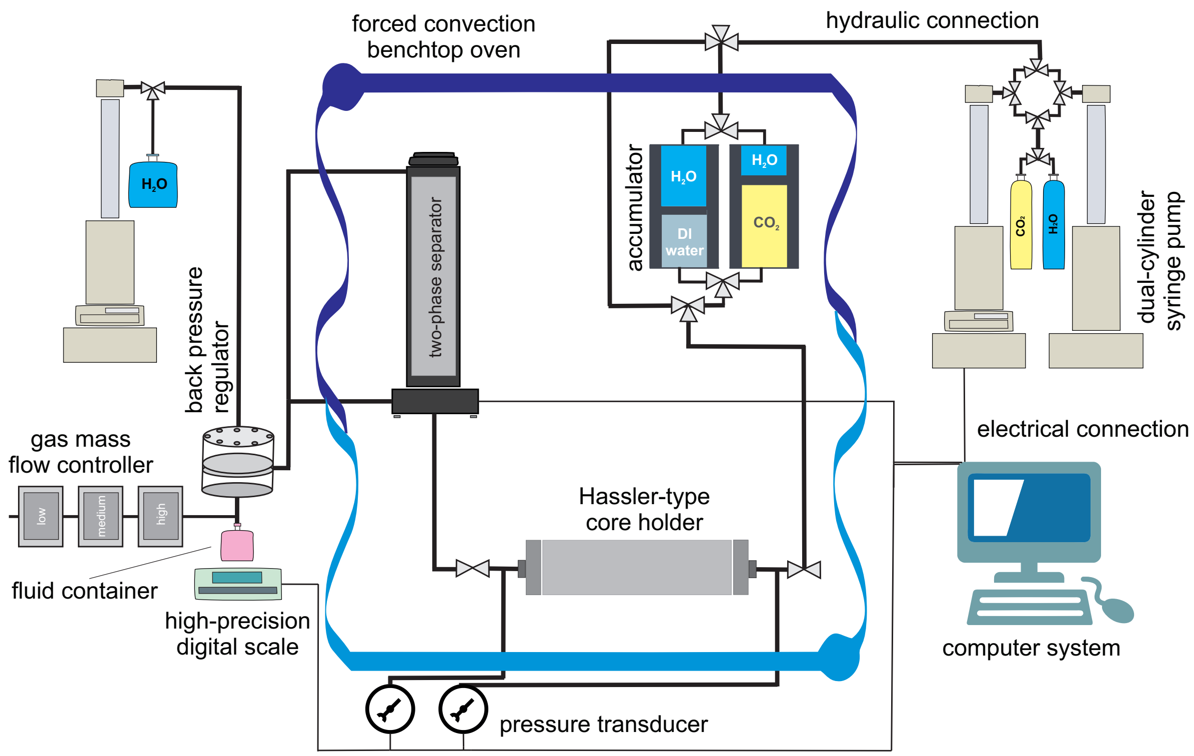

Figure 1. A schematic representation of the high-pressure high-temperature core-flooding system used in the flow-through experiments, modified from Nooraiepour et al. (2018b).

Relative permeability measurements

To make sure that no air or other fluids were entrapped inside the core plug, we initially saturated the sample with DI-water inside a vacuum chamber. The core plug was subsequently placed into the core sleeve inside the core holder. Special care was taken by wrapping the core plug inside an aluminum foil to prevent CO_2 diffusion through the rubber sleeve. The pressure offset of the pressure transducers was corrected by opening the connections to the atmospheric pressure before each experiment. The length of the core plug (about 72 mm) was considered long enough to minimise capillary end effects.

The unsteady-state drainage relative permeability curves were measured by setting 3 MPa backpressure and injection of gaseous CO_2 at a constant rate of 0.1 cm^3/min. Because of the low permeability of the core sample, a low CO_2 injection rate was used to avoid pressure build-up and potential fracture reactivation. The total injected volume of CO_2, total produced water from the core and the observed pressure drop across the core were continuously monitored and logged during the core-flooding experiment. The fluid displacement was continued until recovery of the displaced fluid at the outlet became insignificant. The core inlet was equipped with a one-way check valve to prevent potential back-flow of the in situ pore fluid. The same procedure was followed during the imbibition cycle, in which DI-water displaced the gaseous CO_2. During the imbibition cycle, the water injection rate was reduced to 0.05 cm^3/min to prevent sudden pressure build-up. Because the utilised core holder in this study was not equipped with in situ saturation measurement tools, such as acoustic or computed tomography equipment, irreducible water saturation (S_{wi}) was measured by weighing the core sample after the test. The trapped CO_2 saturation (S_{CO2t}) after the imbibition cycle was determined by calculating the difference between the observed water saturation at this stage and after the drainage cycle. After finishing the relative permeability (k_r) measurements, the core sample was placed under vacuum and, subsequently, the absolute permeability to DI-water (k_a) was measured. The measured ka after the test showed no notable difference compared to the initially measured permeability (Δk_a < 2%). The fractional flow diagrams and the relative permeability curves were interpreted using the methodology suggested by Welge (1952) and Koederitz et al. (1989). The viscosity of DI-water and CO_2 used to estimate permeability were 1.0 and 0.017 cp, respectively (Lemmon et al., 2011).

Results

Characterisation of core properties

Table 1 presents the mineralogical composition and porosity of the tested sample. The bulk mineralogical composition comprised mainly quartz, clay minerals,

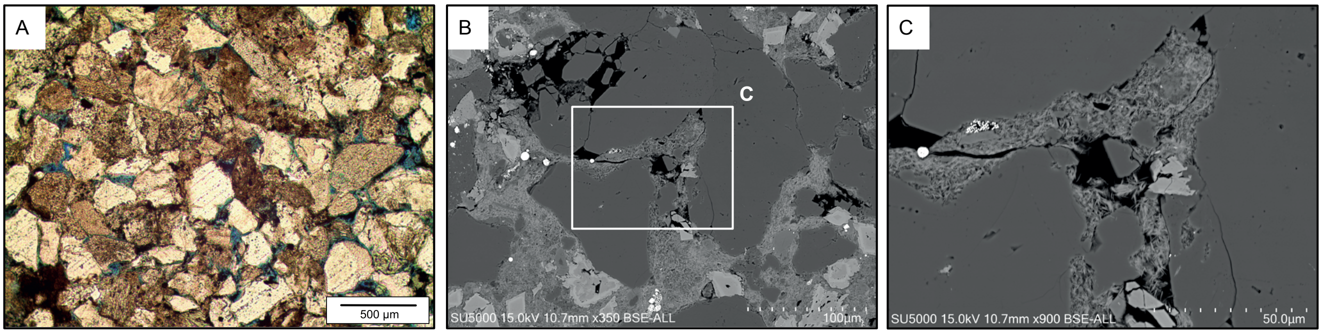

Figure 2. Micrographs of the studied Brentskardhaugen Bed sandstone. (A) Optical micrograph of cemented low-permeability sandstone with rounded to subrounded grains and poor or moderate grain sorting. Light – detrital quartz with quartz cement; darker areas – rock fragments and feldspars; blue – porosity. (B) SEM micrograph of the sample; the boxed region is expanded in C. (C) The presence of clay minerals inside the pore space enclosing secondary dissolution pores may suggest remains of the coated grains and pore-filling clays.

siderite and feldspars and classified as a subarkosic arenite. The clay mineral assemblages consist mainly of chloritic fractions (Table 1). A total porosity of 10.5 was recorded for the sample. The high content of siderite (11.30%) occurs as diagenetic cement which is common in the Brentskardhaugen Bed as shown by Mørk (2013). Optical micrographs and electron microscopy of the tested sample are presented in Figure 2. These show rounded to subrounded grains with poor to moderate grain sorting. The mixed and patchy cement has caused a heterogeneous porous medium inside the sample (Fig. 2). Moreover, the presence of clay minerals enclosing secondary dissolution pores may suggest remains of the coated grains (Mørk, 2013). The clay mineral coatings might play an important role in preserving porosity of the layer when we consider the burial history of the Wilhelmøya Subgroup in western central Spitsbergen. However, extensive quartz and carbonate cements and the presence of clay minerals in the pore spaces and along the pore throats are expected to notably obliterate the permeability of the sample (Fig. 2).

Stress dependence of absolute permeability

The experimental results for absolute permeability of gaseous CO_2 and DI-water are plotted in linear scale as a function of confining and differential pressures in Figure 3. The differential pressure is the difference between confining pressure and pore pressure. Figure 3 demonstrates a power law ($y = a*x^b$) decrease of absolute permeability with the increase of confining and differential pressure at a given pore pressure. The measured permeability decreased from 0.039 to 0.022 mD as the confining pressure increased from 6 to 16 MPa. Moreover, an increase in pore pressure caused an increase in measured permeability. The core-flooding experiments show microDarcy permeability values for various differential pressures (Fig. 3B). A more thorough investigation of the absolute permeability for the Wilhelmøya Subgroup sample has been given by Moghadam et al. (2016).

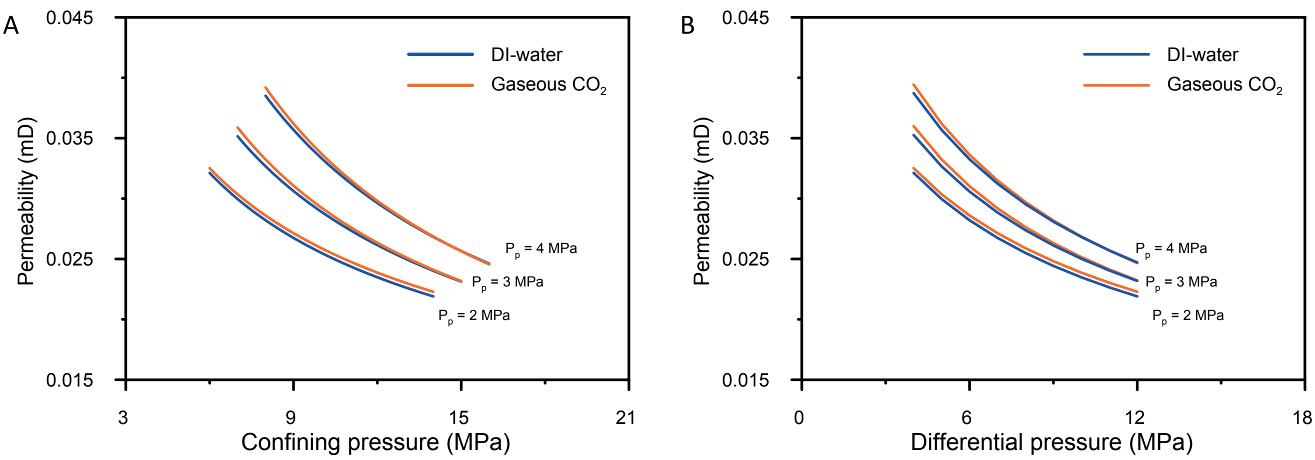

Figure 3. Matrix permeability measurements using gaseous CO_2 and DI-water for a range of (A) Confining and (B) Differential pressures. The measurements were performed at 2, 3 and 4 MPa pore pressure (Pp) levels, modified from Moghadam et al. (2016).

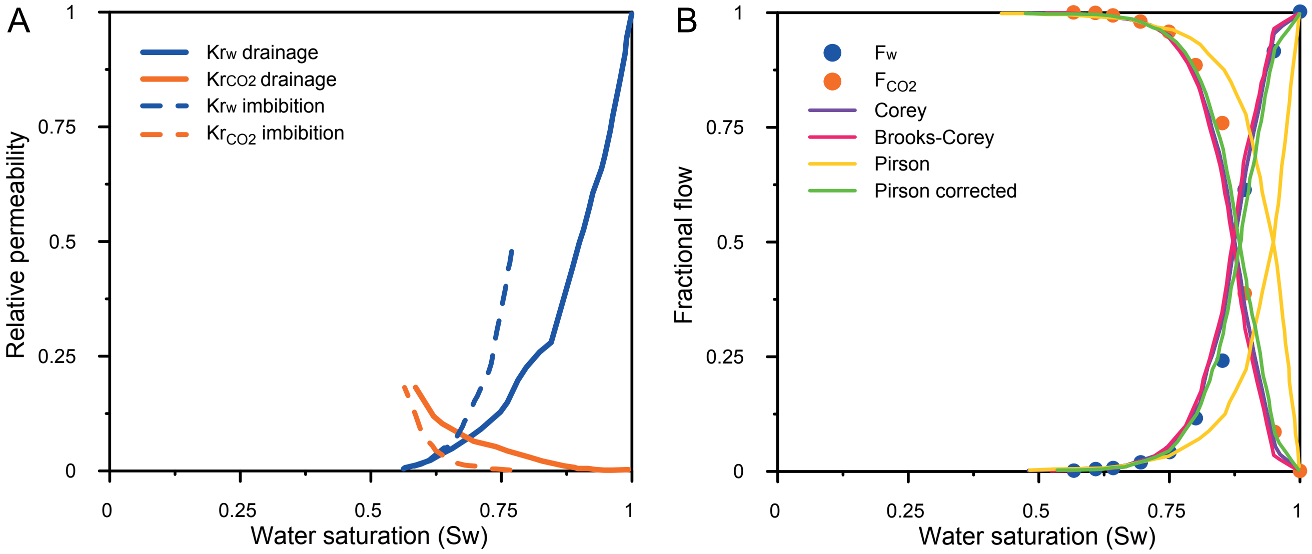

Figure 4. *Unsteady-state two-phase (A) Relative permeability and (B) Fractional flow of the deionised water-gaseous CO_2 system for the Brentskardhaugen Bed (Knorringfjellet) core sample.*

Relative permeability curves

Laboratory investigation of unsteady-state, two-phase, relative permeability of the deionised water-gaseous CO_2 system for the Brentskardhaugen Bed sample is illustrated in Figure 4A. The observed fractional flow of DI-water (f_w) and gaseous CO_2 (f_{CO2}) at the core outlet are presented in Figure 4B. The experimental measurements for the Berea sandstone (the reference core sample in this study) are given in the Appendix. Figure 4 shows that introducing a small amount of CO_2 into the core plug results in a significant reduction in k_{rw}. Moreover, experimental measurements demonstrate that f_{CO2} achieved unity at relatively low CO_2 saturation ($0.35 < S_{CO2} < 0.45$). The irreducible water saturation (S_{wi}) at the end of the drainage is equal to 0.56 after injection of several CO_2 pore volumes when no further production of pore water is detected (Fig. 4). The maximum CO_2 saturation during drainage is correspondingly 0.44. The calculated CO_2 endpoint relative permeability (k_{rCO2}) at the maximum CO_2 saturation S_{CO2m} is 0.18 while the calculated k_{rw} is almost zero. It should be noted that the observed S_{wi} is different from the assigned ultimate S_{wi} (S_{wiu}), in which we assume very high injection pressure to overcome capillary pressure. Due to lack of experimental ultimate irreducible water saturation (S_{wiu}) (Hou et al., 2011), $S_{wiu} = 0.25$ is considered to provide the best-fitting relative permeability models. The ultimate k_{rCO2} at $S_{wiu} = 0.25$ according to the Brook-Corey correlation for finding the best-fitting model was considered to be 0.58 for the Brentskardhaugen Bed sample.

The experimental k_r curves illustrate a strong permeability hysteresis for the drainage and imbibition cycles, in particular for CO_2 (Fig. 4). The trapped CO_2 saturation (S_{CO2t}) at the end of the imbibition is equal to 0.23. At $S_{CO2t} = 0.23$ at the endpoint saturation during the imbibition cycle, the calculated k_{rw} for the Brentskardhaugem Bed core plug is 0.47 while the k_{rCO2} approaches zero.

Figure 5 presents the measured k_r values during drainage and imbibition cycles in addition to the several published relative permeability models. In this study, we used the Corey (Corey, 1954), Brooks and Corey (Brooks & Corey, 1964, 1966) and Pirson (1958) correlations to describe the laboratory relative permeability measurements. These correlations use saturation and permeability endpoint data to model k_r values for the whole saturation interval. To provide the best-fitting k_r models and find the appropriate model coefficients, we applied nonlinear multivariate regression to the experimental measurements. Table 2 summarises the applied regression parameters for

Table 1. *Calculated k_r correlation coefficients for the tested core plugs during drainage and imbibition cycles.*

Displacement cycle	*Drainage*				*Imbibition*			
k_r correlation coefficient	*Brook & Corey*		*Pirson (Corrected)*		*Brook & Corey*		*Pirson (Corrected)*	
	n_w	n_{CO2}	$\alpha_w^{\ d}$	$\alpha_{CO2}^{\ d}$	n_w	n_{CO2}	$\alpha_w^{\ i}$	$\alpha_{CO2}^{\ i}$
Knorringfjellet	5.07	2.55	6.34	1.31	2.78	0.54	3.28	4.22
Berea	5.22	4.20	6.53	1.44	1.90	0.84	4.82	3.28

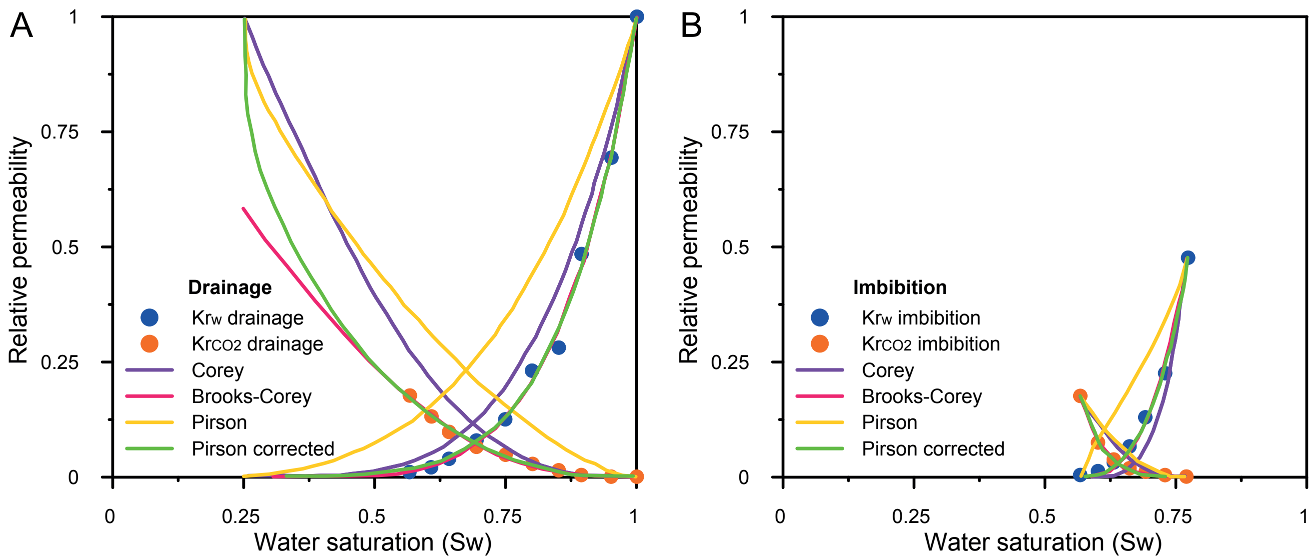

Figure 5. *(A) Drainage and (B) Imbibition relative permeability curves for the Brentskardhaugen Bed (Knorringfjellet) core sample, in addition to several published relative permeability models. The Pirson correlation (Pirson, 1958) was modified to provide a best-fitting model for the studied sample.*

modelling the measured relative permeability data. As illustrated in Figure 5, during drainage, Corey and Pirson's correlations overpredict k_r values for both DI-water and gaseous CO_2. After correction of the mentioned k_r correlations by considering suitable fitting parameters ($n_w = 5.07$, $n_{CO2} = 2.55$ $\alpha_w{}^d = 6.34$ and $\alpha_{CO2}{}^d = 1.31$) in the form of the generalised Brook and Corey and corrected Pirson's correlation, they provide more consistent k_r estimates for the laboratory observations. For the imbibition cycle, Corey's correlation underestimates k_{rw} values, and the Pirson's derived-k_{rCO2} is significantly overestimated. The corrected Corey and Pirson's correlations ($n_w = 2.78$, $n_{CO2} = 0.54$, $\alpha_w{}^i = 3.28$ and $\alpha_{CO2}{}^i = 4.22$) provided model predictions that fit well with the experimental values for the Brentskardhaugen Bed core sample.

In addition, we used the above-described models to calculate the fractional flow for each correlation. As shown in Figure 4, all of the plotted k_r models except Pirson's correlation have provided model predictions that are in good agreement with the experimental f_w and f_{CO2}. The Pirson's correlation could provide better estimates for fractional flow using the given coefficients in Table 2 (Fig. 4).

Discussion

Roles of fractures in permeability of the Wilhelmøya Subgroup

An extensive mapping of the fracture networks in the LYBCO$_2$ reservoir and seal units have been reported in Ogata et al. (2014a, b). Here, the Brentskardhaugen Bed was mechanically classified together with other massive to laminated, thick-bedded, medium- to coarse-grained intervals. This unit is dominated by high-angle systematic bed-confined and through-going fractures, with subordinate low-angle fractures (Ogata et al., 2014b). The fracture spacing was found to have a log-normal distribution with a median distance of 10 cm. We have to keep in mind that the high-resolution CT scans from the same units have revealed an increasing number of observed microfractures with increasing spatial resolution (Van Stappen et al., 2014).

The permeabilities measured at the lowest confining stresses at 6–8 MPa are in the lowermost range of earlier values measured in this interval at approximately 674 m depth in the Wilhelmøya Subgroup in the DH 4 well (Farokhpoor et al., 2010). It is clear that increasing confining pressure leads to an exponential decrease in permeabilities, demonstrating that fracture closing has a main controlling effect on the permeabilities (Van Stappen et al., 2018; present study), also for samples with sub-micron fractures that were not detected petrographically or by SEM (present study). The reduction of permeability by increasing the confining pressure from 1 to 10 MPa has been shown to reduce the permeability by more than 90% (Van Stappen et al., 2018). Our measured permeabilities appear to converge towards ~0.02 mD with increasing confining pressures and effective stresses. This is somewhat higher than the non-fractured field samples examined by Van Stappen et al. (2018) (<0.01 mD). Local variations caused by the heterogeneous distribution of cements and corresponding differences in matrix permeability are, however, to be expected (Farokhpoor et al., 2010). There is no information on the confining pressure used in Farokhpoor et al. (2010), but low confining pressures and dominance of fracture flow may be the reason for the high permeability values given in the former publications. Well injection tests and modelling of the pressure fall-off curves also suggest that fracture networks with approximately 2 mD permeability are responsible for the flow in the Wilhelmøya Subgroup (Mulrooney et al., in press). Earlier interpretations of falloff data (Larsen, 2010, 2012) suggest that the main flow is a function of matrix permeability, but this is not likely given the measured permeabilities of the non-fractured rocks, or for samples run at high confining pressures.

Interpretation of relative permeability curves

Because the injected gaseous CO_2 has a low viscosity ($\mu_{CO2} \approx 0.017$ cp), the water-CO_2 system for the Brentskardhaugen Bed sample can be considered as high mobility with limited gravity segregation. In addition, capillary forces further decrease the gravity segregation effect (Krevor et al., 2012; Ruprecht et al., 2014). Thus, since we performed horizontal core-flooding experiments, the impact of gravity segregation on relative permeability measurements is negligible.

Characteristics of the relative permeability curve in Figure 4, such as endpoint saturations, endpoint permeabilities and the crossover points, suggest a water-wetting nature for the Brentskardhaugen Bed sample (Bultreys et al., 2016). In a water-wet porous medium, while the non-wetting fluid (CO_2) is expected to occupy larger pores, the wetting agent (water) is expected to fill smaller pores. As a result, in low-permeability and heterogeneous cemented samples, fluid flow will take place just in a small fraction of the matrix pore space. Therefore, the increase of CO_2 saturation leads to pore water discontinuity and a rapid decrease in k_{rw} (Fig. 4). A similar observation for the Knorringfjellet core samples was reported by Farokhpoor et al. (2012) and Bultreys et al. (2016). The 'Permeability Jail' model (Cluff & Byrnes, 2010) can be used to explain two-phase gas–water relative permeability in tight sandstone reservoirs. The rapid decrease in k_{rw} and a saturation region in which the relative permeabilities to both gaseous CO_2 and water are low (Fig. 4) happens because each fluid phase blocks the other from moving within the pore space. The previously published endpoint measurements for a Wilhelmøya Subgroup (Knorringfjellet) core sample with 10% porosity shows $S_{wi} = 0.60$ and $k_{rCO2} = 0.30$ (Farokhpoor et al., 2012), which is in agreement with the results of the present study. The low endpoint k_{rCO2} can be attributed to CO_2 channelling and fingering because of the existence of rock heterogeneity and unfavourable low CO_2 viscosity. Moreover, displacing water with low-viscosity CO_2 results in poor sweep efficiency, early breakthrough, and high f_{CO2} at relatively high water saturation (Fig. 4). Because there is a significant contrast between water and CO_2 viscosities ($\mu_{water}/\mu_{CO2} \approx 59$), the viscous forces are very low in this water-CO_2 system. When viscous forces are low and water-CO_2 interfacial tension is high, the capillary pressure that is necessary for reaching higher CO_2 saturations cannot be achieved, and it leads to a low endpoint k_{rCO2}. However, the low k_{rCO2} and S_{CO2} in water-CO_2 systems may not be considered as ultimate endpoint values unless sufficient capillary pressure is achieved during the experiment (Krevor et al., 2012).

Li et al. (2012) have shown that in water-CO_2 systems, interfacial tension of gaseous CO_2 is higher than the supercritical CO_2 ($scCO_2$). Considering the lower viscosity and higher interfacial tension of gaseous CO_2 compared with $scCO_2$, it is expected that capillary forces dominate the viscous forces in fluid flow. Consequently, a lower k_{rCO2} for gaseous CO_2 is expected compared to $scCO_2$.

Comparison of experimental results for the tight Brentskardhaugen Bed sample and the reference Berea sandstone core plug (see Appendix) shows that, despite higher absolute permeability of the Berea Sandstone, the observed endpoint k_{rCO2} and S_{CO2} after the drainage process is higher for the Brentskardhaugen Bed sample. A similar observation was also previously reported by Bennion & Bachu (2005), in which the k_{rCO2} and S_{CO2} for the low-permeability Basal Cambrian sandstone plug were higher than in the high-permeability Viking sandstone. In the case of the low-permeability sample, the narrower scatter of pore size distribution may result in a lower CO_2 bypassing some portions of the pore space, and consequently, a higher endpoint k_{rCO2}. A potential wettability difference between the two sandstones also influences the endpoint properties.

CO_2 residual trapping

Because of the discontinuity of the CO_2 phase during the imbibition process, CO_2 will be trapped as an immobile portion inside the water phase. To investigate saturation of residual trapped CO_2 (S_{CO2t}) after injection of several pore volumes of water (during imbibition), we used Land's trapping model (Land, 1968). The Land trapping model provides a relationship between the maximum saturation of the non-wetting phase at the end of the drainage (S_{nwm}) and the trapped saturation of the non-wetting phase at the end of the imbibition (S_{nwt}). According to Land (1968), we expect that d_{SCO2t}/d_{SCO2m} will be > 0. In another words, the higher the $S_{CO2}m$ during the drainage the higher the trapped CO_2 saturation. The higher CO_2 entrapment of the Brentskardhaugen Bed sample ($S_{CO2t} = 0.23$) compared with Berea ($S_{CO2t} = 0.20$) after the imbibition can thus be attributed to the higher CO_2 saturation (S_{CO2m}) of the former during the drainage cycle. Bultreys et al. (2016) also showed that the Knorringfjellet sandstones have higher trapping efficiencies than the samples with well-connected macropores. The proportionality of observed S_{CO2t} and achieved $S_{CO2}m$ has previously been documented (Bennion & Bachu, 2010; Ruprecht et al., 2014). Land's trapping coefficient (C_L) for the Brentskardhaugen

Bed sample shows a higher CO_2 entrapment capability compared with Berea. The experimental results demonstrate that a large portion of the injected CO_2 ($0.20 < S_{CO2t} < 0.25$) might be trapped inside the pore space after performing just one drainage-imbibition cycle. It may provide an experimental indication of the practicality of a CO_2 residual trapping mechanism for the studied sample. The previous studies have also reported that a considerable amount of the injected CO_2 can be immobilised in the Brentskardhaugen Bed ($0.20 < S_{CO2t} < 0.25$) and Berea ($0.21 < S_{CO2t} < 0.40$) sandstones (Juanes et al., 2006; Pentland et al., 2011; Shi et al., 2011; Farokhpoor et al., 2012; Van Stappen et al., 2014; Bultreys et al., 2016).

Implications for CO_2 storage in low-permeability sandstones

The present research provides experimental insights for CO_2 storage in chemically compacted sandstones such as the aquifers in a pilot project UNIS CO_2 LAB or the Barents Sea. The cemented sandstone reservoirs such as the Wilhelmøya Subgroup in Svalbard and in the deeper or previously deeper buried parts of the offshore counterpart, the Realgrunnen Subgroup in the Barents Sea, are characterised by moderate porosity and very low matrix permeability (Mørk, 2013). While fracture networks inside the Upper Triassic–Mid dle Jurassic reservoirs serve as primary fluid-flow conduits (Braathen et al., 2012; Ogata et al., 2014a), the porous medium inside the matrix of the Wilhelmøya Subgroup sandstones provides the storage volume for the injected CO_2. The higher fracture permeability compared with the matrix permeability of these reservoirs (Nooraiepour et al., 2018a) brings about a faster distribution of injected fluid and injection-induced pressure. Because of the low matrix permeability, a slow interaction between the fracture and the surrounding matrix block is expected. Moreover, the low sweep efficiency of the water-CO_2 system leads to high residual water saturation, and low endpoint CO_2 saturation and relative permeability. The lower k_{rCO2} for gaseous CO_2 compared to $scCO_2$ suggests that in the case of under-pressured reservoirs such as the Longyearbyen reservoir units at about 50 bar underpressure (Braathen et al., 2012; Bohloli et al., 2014), we may expect a poor displacement efficiency. On the other hand, the higher CO_2 entrapment capability of the low-permeability Brentskardhaugen Bed sandstone compared with the high-permeability Berea sandstone after performing just one drainage-imbibition cycle provides promising results regarding CO_2 residual trapping in sandstones belonging to the Wilhelmøya Subgroup reservoir units.

Conclusions

In this study, we performed two-phase, unsteady-state, relative permeability measurements of the deionised water-CO_2 system for a low-permeability sandstone sample from the Brentskardhaugen Bed of the Wilhelmøya Subgroup, western central Spitsbergen, Svalbard. The poor grain sorting and abundance of cement and ductile minerals resulted in a heterogeneous and tortuous porous medium, which contributed to the low matrix permeability of the sample. The core-flooding experiments showed microDarcy permeability values for various differential pressures that range between 0.022 and 0.039 mD. It is also likely that submicron fractures are becoming closed as a result of increasing effective stresses, and, thus, leading to even lower permeabilities. The unsteady-state water-CO_2 flooding experiments showed that CO_2 could displace 44% (S_{CO2m}) of the wetting phase (water) during drainage. The calculated CO_2 endpoint relative permeability (k_{rCO2}) at S_{CO2m} was 0.18. The trapped CO_2 saturation (S_{CO2t}) was 23% at the end of imbibition where endpoint k_{rw} reached 0.47. The Brentskardhaugen Bed core sample showed a higher trapped residual CO_2 saturation and higher endpoint k_{rCO2} compared with the porous and permeable Berea sandstone.

The observed endpoint S_{CO2} and k_{rCO2} for gaseous CO_2 were relatively low because of the domination of capillary forces over the viscous forces in the water-CO_2 system. Moreover, the relatively high fractional flow of CO_2 was observed at high water saturation due to unfavourable mobility contrast between water and CO_2, and the resulting low sweep efficiency of the pore water. A lower k_{rCO2} for gaseous CO_2 was recorded compared with published relative permeability curves for $scCO_2$. The difference was attributed to the lower viscosity and higher interfacial tension of gaseous CO_2 compared to $scCO_2$, which causes capillary forces to dominate the viscous forces.

The snap-off phenomenon or CO_2 discontinuity and trapping in larger pores with the water-wet porous medium of the Brentskardhaugen Bed sample is believed to be the main reason for the high percentage of trapped CO_2 after imbibition. The high magnitude of trapped S_{CO2} because of the hysteresis phenomenon provides an experimental indication for the significance of residual trapping mechanism in immobilising the injected CO_2, particularly at the early stages of CO_2 sequestration.

Acknowledgements. The authors would like to thank the Research Council of Norway (Norges Forskningsråd) for funding FME SUCCESS Centre (subsurface CO_2 storage — critical elements and superior strategies). We appreciate CO_2 Field Laboratory at the University Centre in Svalbard (UNIS) for providing the core sample. We are grateful to two anonymous reviewers for their constructive and helpful comments on the manuscript.

References

Akbarabadi, M. & Piri, M. 2013: Relative permeability hysteresis and capillary trapping characteristics of supercritical CO_2/brine systems: An experimental study at reservoir conditions. *Advances in Water Resources 52*, 190–206. https://doi.org/10.1016/j.advwatres.2012.06.014.

Bennion, B. & Bachu, S. 2005: Relative Permeability Characteristics for Supercritical CO_2 Displacing Water in a Variety of Potential Sequestration Zones. *SPE Annual Technical Conference and Exhibition, 9–12th October, Society of Petroleum Engineers, Dallas, Texas*, p. 15. https://doi.org/10.2118/95547-MS.

Bennion, D.B. & Bachu, S. 2010: Drainage and Imbibition CO_2/Brine Relative Permeability Curves at Reservoir Conditions for High-Permeability Carbonate Rocks. *SPE Annual Technical Conference and Exhibition, 19–22nd September, Society of Petroleum Engineers, Florence, Italy,* p. 18. https://doi.org/10.2118/134028-MS.

Benson, S.M., Pini, R., Reynolds, C. & Krevor, S. 2013: Relative permeability analysis to describe multi-phase flow in CO_2 storage reservoirs. *Global CCS Institute Special Report,* 1–51.

Bohloli, B., Skurtveit, E., Grande, L., Titlestad, G.O., Børresen, M.H., Johnsen, Ø., Braathen, A. & Braathen, A. 2014: Evaluation of reservoir and cap-rock integrity for the longyearbyen CO_2 storage pilot based on laboratory experiments and injection tests. *Norwegian Journal of Geology 94*, 171–187.

Braathen, A., Bælum, K., Christiansen, H.H., Dahl, T., Eiken, O., Elvebakk, H.K., Hansen, F.S., Hanssen, T.H., Jochmann, M., Johansen, T.A., Johnsen, H., Lie, T., Mertes, J.R., Larsen, L., Mørk, A., Mørk, M.B.E., Nemec, W., Olaussen, S., Oye, V., Rød, K., Titlestad, G.O., Tveranger, J. & Vagle, K. 2012: The Longyearbyen CO_2 Lab of Svalbard, Norway — initial assessment of the geological conditions for CO_2 sequestration *Norwegian Journal of Geology 92*, 353–376.

Brooks, R.H. & Corey, A.T. 1964: Hydraulic properties of porous media and their relation to drainage design. *Transactions of the American Society of Agricultural Engineers 7*, 26–28. https://doi.org/10.13031/2013.40684.

Brooks, R.H. & Corey, A.T. 1966: Properties of porous media affecting fluid flow. *Journal of the Irrigation and Drainage Division 92*, 61–90.

Bultreys, T., Stappen, J.V., Kock, T.D., Boever, W.D., Boone, M.A., Hoorebeke, L.V. & Cnudde, V. 2016: Investigating the relative permeability behavior of microporosity-rich carbonates and tight sandstones with multiscale pore network models. *Journal of Geophysical Research: Solid Earth 121*, 7929–7945. https://doi.org/10.1002/2016JB013328.

Burnside, N.M. & Naylor, M. 2014: Review and implications of relative permeability of CO_2/brine systems and residual trapping of CO_2. *International Journal of Greenhouse Gas Control 23*, 1–11. https://doi.org/10.1016/j.ijggc.2014.01.013,

Bäckström, S.A. & Nagy, J. 1985: Depositional history and fauna of a Jurassic phosphorite conglomerate (the Brentskardhaugen Bed) in Spitsbergen. *Norsk Polarinstitutt Skrifter 183*, 1–61.

Chen, X., Kianinejad, A. & DiCarlo, D.A. 2014: An Experimental Study of CO_2-Brine Relative Permeability in Sandstone. *SPE Improved Oil Recovery Symposium, 12–16th April, Society of Petroleum Engineers, Tulsa, Oklahoma,* p. 14. https://doi.org/10.2118/169137-MS.

Chen, X., Gao, S., Kianinejad, A. & DiCarlo, D.A. 2017: Steady-state supercritical CO_2 and brine relative permeability in Berea sandstone at different temperature and pressure conditions. *Water Resources Research 53*, 6312–6321. https://doi.org/10.1002/2017WR020810.

Civan, F. 2010: Effective correlation of apparent gas permeability in tight porous media. *Transport in Porous Media 82*, 375–384. https://doi.org/10.1007/s11242-009-9432-z.

Cluff, R.M. & Byrnes, A.P. 2010: Relative Permeability In Tight Gas Sandstone Reservoirs - The "Permeability Jail" Model. *SPWLA 51st Annual Logging Symposium, 19–23rd June, Society of Petrophysicists and Well-Log Analysts, Perth, Australia*, p. 16.

Corey, A.T. 1954: The interrelation between gas and oil relative permeabilities. *Producers monthly 19*, 38–41.

Doughty, C. 2007: Modeling geologic storage of carbon dioxide: Comparison of non-hysteretic and hysteretic characteristic curves. *Energy Conversion and Management 48*, 1768–1781. https://doi.org/10.1016/j.enconman.2007.01.022.

Farokhpoor, R., Torsater, O., Baghbanbashi, T., Mork, A. & Lindeberg, E.G.B. 2010: Experimental and Numerical Simulation of CO_2 Injection Into Upper-Triassic Sandstones in Svalbard, Norway. *SPE International Conference on CO_2 Capture, Storage, and Utilization, 10–12th November, Society of Petroleum Engineers, New Orleans, Louisiana,* p. 11.

Farokhpoor, R., Lindeberg, E.G.B., Mørk, M.B.E., Torsæter, O. & Mørk, A. 2012: CO_2-Brine Relative Permeability Characteristics of Low Permeable Sandstones in Svalbard. *International Symposium-Society of Core Analysts, 27–30th August, Aberdeen, Scotland*, p. 6.

Hou, J., Luo, F., Wang, C., Zhang, Y., Zhou, K. & Pan, G. 2011: Quantitative Prediction Model for the Water–Oil Relative Permeability Curve and Its Application in Reservoir Numerical Simulation. Part 1: Modeling. *Energy & Fuels 25*, 4405–4413.

Iding, M. & Ringrose, P. 2010: Evaluating the impact of fractures on the performance of the In Salah CO_2 storage site. *International Journal of Greenhouse Gas Control 4*, 242–248. https://doi.org/10.1016/j.ijggc.2009.10.016.

Juanes, R., Spiteri, E.J., Orr, F.M. & Blunt, M.J. 2006: Impact of relative permeability hysteresis on geological CO_2 storage. *Water Resources Research 42*. https://doi.org/10.1029/2005WR004806.

Klinkenberg, L.J. 1941: The permeability of porous media to liquids and gase. *API Drilling and Production Practice, 1st January, New York, New York,* p. 14.

Koederitz, L., Harvey, A.H. & Honarpour, M. 1989: *Introduction to Petroleum Reservoir Analysis Laboratory Workbook*. Gulf Publishing Company, Book Division, 250 pp.

Krevor, S.C.M., Pini, R., Zuo, L. & Benson, S.M. 2012: Relative permeability and trapping of CO_2 and water in sandstone rocks at reservoir conditions. *Water Resources Research 48*.

Land, C.S. 1968: Calculation of imbibition relative permeability for two-and three-phase flow from rock properties. *Society of Petroleum Engineers Journal 8*, 149–156. https://doi.org/10.2118/1942-PA.

Larsen, L. 2010: Analyses of Injection and Falloff Data from DH4, Aug.12–Sept. 4, 2010. *Longyearbyen CO_2 Lab UNIS Unpublished Report.*

Larsen, L. 2012: Analyses of Sept. 2011 Upper Zone Injection and Falloff Data from DH6 and Interference Data from DH5. *Longyearbyen CO_2 Lab UNIS Unpublished Report.*

Lemmon, E.W., McLinden, M.O. & Friend, D.G. 2011: Thermophysical properties of fluid systems. *In* Linstrom, P.J. & Mallard, W.G. (eds.): *NIST chemistry webBook*, NIST Standard Reference Database Number 69, National Institute of Standards and Technology.

Li, X., Boek, E.S., Maitland, G.C. & Trusler, J.P.M. 2012: Interfacial Tension of (Brines + CO_2): $CaCl_2$(aq), $MgCl_2$(aq), and Na_2SO_4(aq) at Temperatures between (343 and 423) K, Pressures between (2 and 50) MPa, and Molalities of (0.5 to 5) mol·kg–1. *Journal of Chemical & Engineering Data 57*, 1369–1375. https://doi.org/10.1021/je300304p.

Magnabosco, C., Braathen, A. & Ogata, K. 2014: Permeability model of tight reservoir sandstones combining core-plug and miniperm analysis of drillcore; Longyearbyen CO_2 lab, Svalbard. *Norwegian Journal of Geology 94*, 189–200.

Moghadam, J.N., Mondol, N.H., Aagaard, P. & Hellevang, H. 2016: Effective stress law for the permeability of clay-bearing sandstones by the Modified Clay Shell model. *Greenhouse Gases: Science and Technology 6*, 752–774.

Moore, J.R., Glaser, S.D., Morrison, H.F. & Hoversten, G.M. 2004: The streaming potential of liquid carbon dioxide in Berea Sandstone. *Geophysical Research Letters 31*. https://doi.org/10.1029/2004GL020774.

Mulrooney, M.J., Van Stappen, J., Cnudde, V., Senger, K., Rismyhr, B., Braathen, A., Olaussen, S., Mørk, M.B. & Ogata, K. in press: Fluid flow properties of a potential unconventional CO_2 storage unit in central Spitsbergen: The Upper to Middle Jurassic Wilhelmøya Subgroup. *Norwegian Journal of Geology XX,* XX–XX. https://dx.doi.org/10.17850/njg002.

Mørk, A., Dallmann, W.K., Dypvik, H., Johannesen, P., Larssen, G.B., Nagy, J., Nøttvedt, A., Olaussen, S., Pcelina, T.M. & Worsley, D. 1999: Mesozoic lithostratigraphy. *In* Dallmann, W.K. (ed.): *Lithostratigraphic atlas of Svalbard*, Norwegian Polar Institute, Tromsø, Norway, pp. 127–214.

Mørk, M.B.E. 2013: Diagenesis and quartz cement distribution of low-permeability Upper Triassic–Middle Jurassic reservoir sandstones, Longyearbyen CO_2 lab well site in Svalbard, Norway. *AAPG Bulletin 97*, 577–596. https://doi.org/10.1306/10031211193.

Nooraiepour, M., Haile, B.G. & Hellevang, H. 2017a: Compaction and mechanical strength of Middle Miocene mudstones in the Norwegian North Sea – The major seal for the Skade CO_2 storage reservoir. *International Journal of Greenhouse Gas Control 67*, 49–59. https://doi.org/10.1016/j.ijggc.2017.10.016.

Nooraiepour, M., Mondol, N.H., Hellevang, H. & Bjørlykke, K. 2017b: Experimental mechanical compaction of reconstituted shale and mudstone aggregates: Investigation of petrophysical and acoustic properties of SW Barents Sea cap rock sequences. *Marine and Petroleum Geology 80*, 265–292. https://doi.org/10.1016/j.marpetgeo.2016.12.003.

Nooraiepour, M., Bohloli, B., Park, J., Sauvin, G., Skurtveit, E. & Mondol, N. 2018a: Effect of brine-CO_2 fracture flow on velocity and electrical resistivity of naturally fractured tight sandstones. *Geophysics 83*, WA37–WA48. https://doi.org/10.1190/geo2017-0077.1.

Nooraiepour, M., Fazeli, H., Miri, R. & Hellevang, H. 2018b: Effect of CO_2 Phase States and Flow Rate on Salt Precipitation in Shale Caprocks—A Microfluidic Study. *Environmental Science & Technology 52*, 6050–6060. https://doi.org/10.1021/acs.est.8b00251.

Oak, M.J., Baker, L.E. & Thomas, D.C. 1990: Three-phase relative permeability of Berea Sandstone. *Journal of Petroleum Technology 42*, 1054–1061. https://doi.org/10.2118/17370-PA.

Ogata, K., Senger, K., Braathen, A., Tveranger, J. & Olaussen, S. 2014a: The importance of natural fractures in a tight reservoir for potential CO_2 storage: A case study of the upper Triassic-middle Jurassic Kapp Toscana Group (Spitsbergen, Arctic Norway). *Geological Society Special Publication 374*, 395–415.

Ogata, K., Senger, K., Braathen, A., Tveranger, J. & Olaussen, S. 2014b: Fracture systems and mesoscale structural patterns in the siliciclastic mesozoic reservoir-caprock succession of the longyearbyen CO_2 lab project: Implications for geological CO_2 sequestration in central spitsbergen, svalbard. *Norwegian Journal of Geology 94*, 121–154.

Pentland, C.H., El-Maghraby, R., Iglauer, S. & Blunt, M.J. 2011: Measurements of the capillary trapping of super-critical carbon dioxide in Berea sandstone. *Geophysical Research Letters 38*. https://doi.org/10.1029/2011GL046683.

Perrin, J.-C. & Benson, S. 2010: An Experimental Study on the Influence of Sub-Core Scale Heterogeneities on CO_2 Distribution in Reservoir Rocks. *Transport in Porous Media 82*, 93–109. https://doi.org/10.1007/s11242-009-9426-x.

Pini, R., Krevor, S.C.M. & Benson, S.M. 2012: Capillary pressure and heterogeneity for the CO_2/water system in sandstone rocks at reservoir conditions. *Advances in Water Resources 38*, 48–59. https://doi.org/10.1016/j.advwatres.2011.12.007.

Pirson, S.J. 1958: *Oil reservoir engineering, 2nd ed.* McGraw-Hill, New York, USA, 735 pp.

Qi, R., LaForce, T.C. & Blunt, M.J. 2009: Design of carbon dioxide storage in aquifers. *International Journal of Greenhouse Gas Control 3*, 195–205. https://doi.org/10.1016/j.ijggc.2008.08.004.

Rinaldi, A.P. & Rutqvist, J. 2013: Modeling of deep fracture zone opening and transient ground surface uplift at KB-502 CO_2 injection well, In Salah, Algeria. *International Journal of Greenhouse Gas Control 12*, 155–167. https://doi.org/10.1016/j.ijggc.2012.10.017.

Ruprecht, C., Pini, R., Falta, R., Benson, S. & Murdoch, L. 2014: Hysteretic trapping and relative permeability of CO_2 in sandstone at reservoir conditions. *International Journal of Greenhouse Gas Control 27*, 15–27. https://doi.org/10.1016/j.ijggc.2014.05.003.

Saadatpoor, E., Bryant, S.L. & Sepehrnoori, K. 2010: New Trapping Mechanism in Carbon Sequestration. *Transport in Porous Media 82*, 3–17. https://doi.org/10.1007/s11242-009-9446-6.

Sand, G., Braathen, A. & Olaussen, S. 2014: Longyearbyen CO_2 lab - tales of research and education. *Norwegian Journal of Geology 94*, 77–82.

Shi, J.Q., Xue, Z. & Durucan, S. 2011: Supercritical CO_2 core flooding and imbibition in Tako sandstone—Influence of sub-core scale heterogeneity. *International Journal of Greenhouse Gas Control 5*, 75–87. https://doi.org/10.1016/j.ijggc.2010.07.003.

Sifuentes, W.F., Giddins, M.A. & Blunt, M.J. 2009: Modeling CO_2 Storage in Aquifers: Assessing the key contributors to uncertainty. *Offshore Europe*, *Society of Petroleum Engineers*, *8–11th September, Aberdeen*, *UK*, p. 13.

Tidwell, V. & Wilson, J. 1999: Permeability upscaling measured on a block of Berea Sandstone: Results and interpretation. *Mathematical Geology 31*, 749–769. https://doi.org/10.1023/A:1007568632217.

Van Stappen, J., de Kock, T., Boone, M.A., Olaussen, S. & Cnudde, V. 2014: Pore-scale characterisation and modelling of CO_2 flow in tight sandstones using X-ray micro-CT; knorringfjellet formation of the longyearbyen CO_2 lab, Svalbard. *Norwegian Journal of Geology 94*, 201–215. https://doi.org/10.1021/acs.est.8b00861.

Van Stappen, J.F., Meftah, R., Boone, M.A., Bultreys, T., De Kock, T., Blykers, B.K., Senger, K., Olaussen, S. & Cnudde, V. 2018: In Situ Triaxial Testing to Determine Fracture Permeability and Aperture Distribution for CO_2 Sequestration in Svalbard, Norway. *Environmental Science and Technology 52*, 4546–4554.

Welge, H.J. 1952: A Simplified Method for Computing Oil Recovery by Gas or Water Drive. *Journal of Petroleum Technology 4,* 1–8. https://doi.org/10.2118/124-G.

Zhang, Y., Kogure, T., Nishizawa, O. & Xue, Z. 2017: Different flow behavior between 1-to-1 displacement and co-injection of CO_2 and brine in Berea sandstone: Insights from laboratory experiments with X-ray CT imaging. *International Journal of Greenhouse Gas Control 66*, 76–84. https://doi.org/10.1016/j.ijggc.2017.09.005.

Appendix

Fluid-flow properties of the Berea sandstone

This section presents experimental results on the fluid-flow properties of the Berea sandstone as a reference core sample in this study. The mineralogical composition and total porosity of the tested Berea sample are given in Table 1. The bulk mineralogy is composed mainly of quartz grains. The absolute permeability of the core plug varies from 100 to 76 mD as differential stress increases from 2 to 14 MPa. The total porosity was 21% for the sample.

Figure 6 shows the two-phase relative permeability curves of the deionised water-CO_2 system for the Berea sandstone. The observed f_w and f_{CO2} at the core outlet are also presented in Figure 6. At the end of drainage cycle, S_{wi} = 0.6, S_{CO2m} = 0.4, and endpoint k_{rCO2} = 0.13 were recorded. The S_{CO2t} at the end of the imbibition was 0.20, and the endpoint k_{rw} was equal to 0.34. The relative permeability results are in agreement with the previously published experiments on the Berea sandstone (Perrin & Benson, 2010; Krevor et al., 2012; Akbarabadi & Piri, 2013; Chen et al., 2017; Zhang et al., 2017).

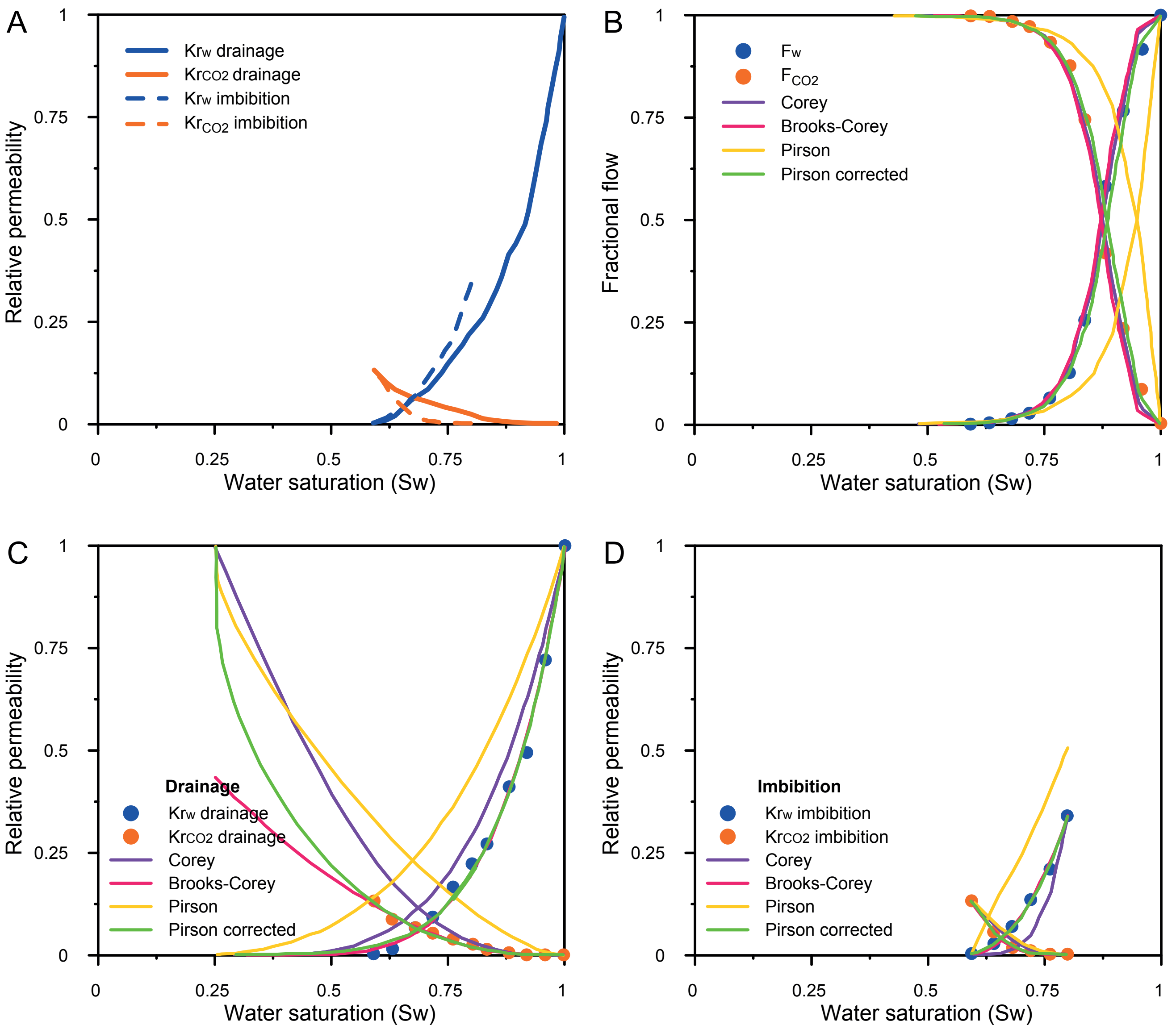

__Figure 6.__ (A) Relative permeability curves and (B) Fractional flow measurements of deionised water-CO_2 system for the Berea sandstone, used as reference material in this study. (C) Drainage and (D) Imbibition relative permeability measurements, in addition to several published relative permeability models. The Pirson correlation (Pirson, 1958) was modified to provide a best-fitting model.